

**RPSEA**

***Final Report***

**08121-2902-03.FINAL**

***Subsea Communications***

**08121-2902-03**

**December 5, 2011**

Daniel Sexton  
Project Engineer  
GE Global Research  
One River Road  
Niskayuna, NY

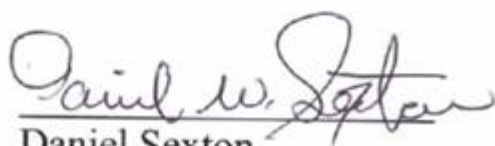
**LEGAL NOTICE**

This report was prepared by The General Electric Company as an account of work sponsored by the Research Partnership to Secure Energy for America, RPSEA. Neither RPSEA members of RPSEA, the National Energy Technology Laboratory, the U.S. Department of Energy, nor any person acting on behalf of any of the entities:

- a. MAKES ANY WARRANTY OR REPRESENTATION, EXPRESS OR IMPLIED WITH RESPECT TO ACCURACY, COMPLETENESS, OR USEFULNESS OF THE INFORMATION CONTAINED IN THIS DOCUMENT, OR THAT THE USE OF ANY INFORMATION, APPARATUS, METHOD, OR PROCESS DISCLOSED IN THIS DOCUMENT MAY NOT INFRINGE PRIVATELY OWNED RIGHTS, OR
- b. ASSUMES ANY LIABILITY WITH RESPECT TO THE USE OF, OR FOR ANY AND ALL DAMAGES RESULTING FROM THE USE OF, ANY INFORMATION, APPARATUS, METHOD, OR PROCESS DISCLOSED IN THIS DOCUMENT.

THIS IS A FINAL REPORT. THE DATA, CALCULATIONS, INFORMATION, CONCLUSIONS, AND/OR RECOMMENDATIONS REPORTED HEREIN ARE THE PROPERTY OF THE U.S. DEPARTMENT OF ENERGY.

REFERENCE TO TRADE NAMES OR SPECIFIC COMMERCIAL PRODUCTS, COMMODITIES, OR SERVICES IN THIS REPORT DOES NOT REPRESENT OR CONSTITUTE AND ENDORSEMENT, RECOMMENDATION, OR FAVORING BY RPSEA OR ITS CONTRACTORS OF THE SPECIFIC COMMERCIAL PRODUCT, COMMODITY, OR SERVICE.

  
Daniel Sexton

12/08/2011  
Date

## **Abstract**

Subsea wireless communications has been accomplished in the past using acoustic and optical technologies. These techniques have significant limitations in real world applications due to noise, interference and water quality conditions (turbidity and fowling). Subsea communications using RF techniques has been investigated but with limited success. This report describes the research efforts into Subsea communications using RF conduction demonstrating that RF conduction presents a viable mechanism for communications through saltwater over short ranges. This project also explored the limits and channel capacity of wireless communications for Subsea operations using RF conduction and demonstrated high speed wireless data transfer in a relevant subsea environment. This project established the basic channel capacity entitlement and then went on to show how modern communications techniques using advanced forms of data modulation and channel coding could significant improve overall performance. One use of this technology is for the communications of collected data from sensors and data loggers on the seabed by remotely guided vehicles.

**THIS PAGE INTENTIONALLY LEFT BLANK**

## **1.1 Introduction**

Subsea wireless communications are accomplished using acoustics, optics, and radio frequency (RF) electromagnetics. Acoustics has limitations in real world applications due to ambient noise and multipath interference, while optics is very susceptible to water quality conditions (turbidity and fowling). Optical waves only deliver good performance in very clear water and require tight alignment of nodes. The requirement for line of sight when using optical communications has imposed a significant constraint on its application in underwater communications.

Most commonly nowadays, both above and underground and water, telecommunication systems are a part of a network. While the attenuation of RF signals is high in conducting media, reliable networks can be formed underwater by using multi-hop and retransmission (Che, et al., 2010). The goal of this project is to explore the limits and capacity of wireless communications for subsea operations using RF conduction. Possible applications range from short range communications ( $< 100\text{m}$ ) which would be appropriate for guidance of Remotely Operated Vehicles (ROVs) and other equipment and very short range ( $< 1\text{m}$ ) very high speed communications for transmission of real time data. This technology can also be used for contactless data transfer between sensor equipped sections of a deep sea drill riser. There is need for contactless data transfer at the riser section joints. Even in that kind of static scenario, line of sight may be lost if one of the elements stops working, thus making RF more suitable than optics. The advantage of RF conduction, as compared to conventional loop antennas, is that the antenna system can be small enough to fit between riser sections. Also, since it does not rely on a resonance or tuned circuits, there is less concern about matching.

In an RF conduction system, increased spacing between electrodes implies higher voltage with same current. That translates into more radiated power with the same current. In (Momma, et al., 1976), the authors state that the effective range is not a function of power but of current. RF conduction antenna system should be designed, for a given application, with optimum size and electrode spacing to give maximum power for the same amount of current.

## **1.2 Technology Status Assessment**

The traditional methods for sub-sea communications are acoustic, optical and low frequency electromagnetic. Some interesting research has also been done demonstrating under-sea radio frequency (RF) communications (Shaw et al 2006). This work, although interesting, has not been corroborated and

## **Subsea Communications Final Report**

### **08121-2902-03**

there is some doubt as to the mechanism of propagation (Somaraju et al 2006). Traditionally, only acoustic and optical communication have provided high enough data rates and distances to support real time monitoring and control of assets using classical approaches. Wired approaches have also been used including conventional twisted pair signaling (RS422, DSL, etc.) as well as power line carrier. However these require connectors capable of being mated in the subsea environment.

Three main techniques are currently available or have been studied for wireless subsea communications; these include optical, acoustic and magnetic/RF. Each of these has advantages and disadvantages.

Optical communications through seawater has significant challenges. Seawater offers a low attenuation to blue/green light in the wavelength range from about 400-500 nanometers as long as the water is clear (Chancey 2005). Blue/Green laser communications has been pursued by the US Navy as a way of communicating with submarines for a number of years. However, in certain parts of the world the water can have turbidity that can occlude even these wavelengths. Bioluminescence, sunlight, and biofouling near the surface can degrade the link fidelity (Chancey 2005). At significant depths the water can be filled with marine snow (organic detritus) that can also scatter these wavelengths or over time accumulate enough to completely block a source or detector if not adequately protected. Motion of assets close to the seabed may also stir up particulate enough to impair propagation of light. However, optical (LED based) transceivers are inexpensive, they have been shown to be able to operate at high data rates (10 Mbps at 140 m) (Chancey 2005, Fair et al, 2006) and with time synchronization between devices can be made to operate at low average power. When combined with mesh routing protocols, a network of these devices can cover a wide area even if single link communications distances are kept small. For maximum efficiency and distance, optical signals should be directed and it is envisioned that an effective optical communications node will have multiple light sources and detectors, limited ability to adjust its position and be able to utilize only those combinations of detectors and sources that yield the best link reliability. Prevention of marine biofouling of the optics still needs to be considered. However, for ultra-deep applications fouling due to marine growth may be less severe because objects are well below the depth of penetration of sunlight (300 m) (DePalma 1962), this may restrict the use of optics to those parts of the operation or below 300m.

Extensive research exists in underwater acoustic networks (Akyildiz 2005). It is known that acoustics suffer some propagation impairments from turbidity (Urlick 1983), but requires less energy per bit than optical communications. Acoustics suffer from long delays which makes mesh protocols, protocols

relying on collision sensing and the use of acknowledgments inefficient. Typical transmission bandwidths have been limited to approximately 10 kHz. The current practical limit for spectral efficiency is approximately 3 bits/s/Hz of carrier bandwidth. This limits the data rate in practical designs to approximately 30 kbps. However, a widely cited study reports 500 kbps at a range of 60 m (Kaya 1989). That suggests a 1 MHz carrier of 125 kHz bandwidth using 16-QAM modulation in a horizontal channel.

Conventional approaches to electromagnetic communications in seawater have been limited to low frequencies because of the depth of penetration, known as skin depth. That is the depth into the material where the loss is 8.68dB. It is not until the period of the electromagnetic wave has decreased below the relaxation time of the material and has also increased beyond where the material dielectric losses are significant that it can be considered for electromagnetic propagation. However, that does not occur until frequencies in the terahertz have been reached (Chaplin).

Over the recent years, a variety of available products for underwater electromagnetic communication has been offered by WFS Technologies, a United Kingdom (UK) based company. They have designed and developed a line of products for data rates 1-100 bps that can perform at ranges out to 30 m. Another one of their line of designs are 25 - 156 kbps systems, optimized for ranges between 2 m and 10 m. WFS Technologies have also been offering an underwater electromagnetic communication system that can transfer up to 1 Mbps at ranges less than 10 m. Their current line of products use loop antennas. The size of their square-shaped loop antenna for high data rates is 25 cm x 15 cm (WFS, 2011).

In (Joe, et al., 2007), based on sea water frequency response obtained by transmitting a 1 us pulse, it was shown that RF conduction method could deliver information at 1 Mbps for binary system. Another article has been published recently about a high-speed underwater RF solution using conduction (Zhiqiang, et al., 2010), where the highest data rate was 1 Mbps at ranges .5 m, 0.8 m and 1 m.

### **1.3 Data Transmission and Reception**

Considering the frequency dependent nature of the electromagnetic field in conducting medium, such as seawater, the Channel Frequency Response (CFR) is not expected to be flat. Therefore, the channel is expected to dissipate more of the transmit power at some frequencies than others. It is also expected that the CFR varies with range. Multi-Carrier (MC) communication is a good approach for that type of channel because it allows

for bit loading and power allocation across individual subcarriers, which can be optimized, provided the CFR is at least approximately known at the transmitter. MC has been successfully used even in extremely time-variable, multipath-interference-rich communication channels such as underwater acoustic communication channel (Stojanovic & Preisig, 2009).

In an MC system, the total available bandwidth  $B$  is divided into  $K$  narrow sub-bands, each of width  $\Delta f = B/K$ . The signal in each sub-band is modulated linearly, using a  $m$ -ary data stream  $d_k$ ;  $k = 0, 1 \dots K-1$ . The modulating signal in the  $k$ -th sub-band of an MC system is given by

$$u_k(t) = d_k e^{j2\pi k \Delta f t} g(t) \quad (1)$$

We refer to  $g(t)$  as the transmitter pulse. In the special case when  $g(t)$  is a rectangular pulse of duration  $T = 1/\Delta f$ , multi-carrier modulation is called Orthogonal Frequency Division Multiplexing (OFDM).

The modulated signal is given by

$$\begin{aligned} s(t) &= \sum_{k=0}^{K-1} \text{Re}\{u_k(t) e^{j2\pi f_0 t}\} \\ &= \text{Re}\{u(t) e^{j2\pi f_0 t}\} \end{aligned} \quad (2)$$

Signal  $u(t)$  in (2) is given by

$$u(t) = \sum_{k=0}^{K-1} u_k(t) \quad (3)$$

When propagation occurs over multiple paths, the received signal (not counting the noise) can be modeled as

$$\bar{r}(t) = \sum_{p=0}^{P-1} h_p s(t - \tau_p) = \text{Re}\{\bar{v}(t) e^{j2\pi f_0 t}\} \quad (4)$$

Coefficients  $h_p$  and  $\tau_p$  are the gain and delay of the  $p$ -th path, respectively, and there are a total of  $P$  propagation paths. It should be noted that, to account for multipath dispersion and reduce intersymbol interference, guard time is typically included in  $u(t)$ . Since our intent on this project was to measure the channel characteristics, and not to implement a full-scale communication system, we excluded the guard time from the experimental waveform analysis.

At the receiver, the (noisy) signal is first demodulated using the carrier frequency  $f_0$ . This process yields the base-band signal

$$v(t) = \bar{v}(t) + w(t) \quad (5)$$

Signal  $w(t)$  in (5) represents the noise. The noise is usually modeled as a zero-mean Gaussian process with independent real and imaginary parts of equal power.

The signal  $v(t)$  is further processed by a bank of filters, such that the output of the  $k$ -th filter is

$$y_k = \int_0^{T_0} v(t) e^{j2\pi k \Delta f t} g(t) dt \quad (6)$$

Here,  $T_0$  represents the duration of the pulse  $g(t)$  in general. In the case of OFDM,  $T_0 = T$ , and

$$g(t) = \begin{cases} A & t \in [0, T] \\ 0 & \text{otherwise} \end{cases}$$

Assuming that the maximal path delay is  $\tau_{\max} \ll T$ , it can be shown that the following holds for an OFDM system:

$$y_k \approx d_k H_k E_g + z_k \quad (7)$$

Constant  $E_g = A^2 T$  is the energy of the pulse  $g(t)$ , and  $z_k$  are independent, identically distributed Gaussian random variables. The coefficients  $H_k$  are determined in terms of the channel gains and delays.

$$H_k = \sum_{p=0}^{P-1} h_p e^{-j2\pi(f_0 + k\Delta f)\tau_p} \quad (8)$$

It is fairly obvious from the respective expressions for  $y_k(t)$  and  $u_k(t)$  that they can be implemented using Discrete Fourier Transform (DFT) and Inverse DFT (IDFT). The size of the IDFT should be chosen as a power of 2, because of the computational efficiency of the Radix-2 FFT algorithms (Proakis, 2007).

For our tests, we designed an OFDM type of communication system that included:

$K = 128$  Subcarriers

Total  $B = 6.25$  MHz

Lowest Frequency = 100 kHz

Subcarrier Spacing = 48.83 kHz

Sampling Frequency = 50 MHz

## Subsea Communications Final Report

### 08121-2902-03

Symbol Duration =  $f_s / B \cdot K = 1024$  samples  
Modulation: BPSK or QPSK on all subcarriers

Data rate that corresponds to this system is:

$$R = K \cdot bpsc \cdot \frac{1}{T} = K \cdot bpsc \cdot \frac{BW}{K} = bpsc \cdot BW \quad (9)$$

Term *bpsc* is introduced to represent number of bits per subcarrier. For BPSK and QPSK, *bpsc* equals to 1 and 2, respectively. Therefore, maximum respective data rates for BPSK and QPSK modulated symbols are 6.25 Mbps and 12.5 Mbps. Note that in a real system there would be guard bands and pilot tones, as well as guard times and channel coding, so a part of the overall bandwidth has to be sacrificed for reliability.

The transmitter was implemented by hard-coding the OFDM symbol waveforms in FPGA, using VHDL code given in Appendix 1.

Preparation for the sea test included MATLAB programming. The code is given in Appendix 2. Post-processing MATLAB code is given in Appendix 3.

It should be pointed out that a disadvantage of OFDM is that peak to average power ratio (PAPR) can be high (Han, et al., 2005). For example, in case of 128 subcarriers, the worst possible PAPR would be  $10\log_{10}128 \approx 21\text{dB}$ . Although it is statistically highly improbable that this PAPR would exceed 10 dB, it would still be a concern in a fully implemented and deployed communication system and we will consider a PAPR reduction method in our research. Since we had a known data set for the experiment, we were able to adjust the transmit data to guarantee that we do not have a PAPR problem.

## 1.4 Hardware Description

Figure 1 represents a block diagram of the transmitter used in the test. It is a completely self-contained unit, battery powered with no connection to the outside world. The waveform generator sends a broadband signal with multiple tones of different frequencies embedded. These waveforms were hard-coded in VHDL and their output controlled by the FPGA. The digital representation of the waveforms is presented to the D/A Converter (DAC), which is then smoothed with a filter and presented to the output driver. The Output Driver is capable of a 1A output current to supply the electrodes. Dynamic range of the DAC component was  $2V_{p-p}$ . The electronics and batteries sufficient to drive the transmitter over several hours (10 NiMH

**Subsea Communications Final Report**  
**08121-2902-03**

batteries) were placed inside a 4 in PVC pipe container which was sealed and water tight to 5 meter depths. The electrodes were small pieces of plugged  $\frac{1}{4}$  in bronze pipe. The separation was set by the mechanical constraints of the package and the length of the electrodes was set so as not to exceed the current drive of the transmitter. The transmitter is capable of producing waveforms up to 10 MHz. A Spartan FPGA was used as the arbitrary waveform generator with clock frequency of 51.6096 MHz.

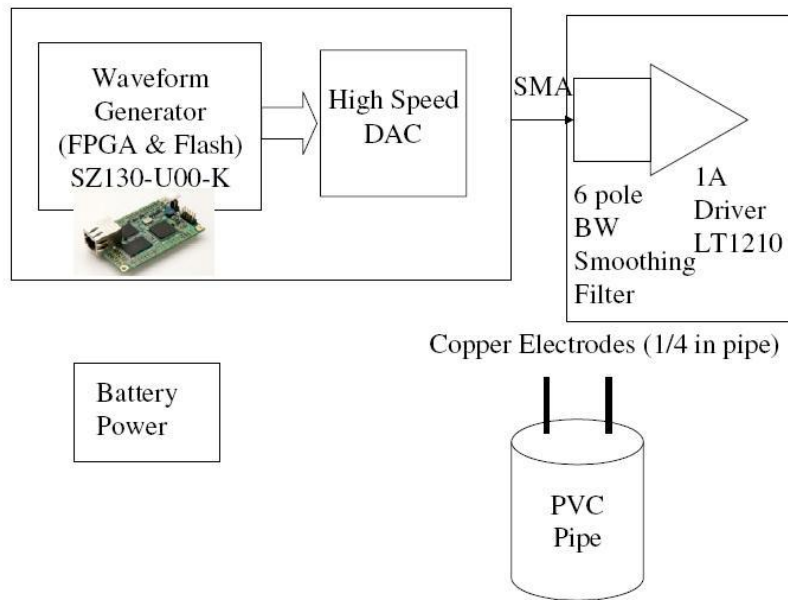


Figure 1 Transmitter diagram.

The receiver utilized a data capture 14 bit acquisition card from Linear Technologies and a Fiber Optic USB connection so that no copper connection was made to the receiver. External 50 MHz clock source was designed and implemented by GE Research. The electronics were battery powered and capable of several hours of operation. A pre-amplifier, model ZFL-1000LN + (15 V) by Mini-Circuits, was included to keep the input signal within range of the ADC (1.5Vp-p). According to the product specifications, the amplifier gain is 23.56 dB across the frequency range.

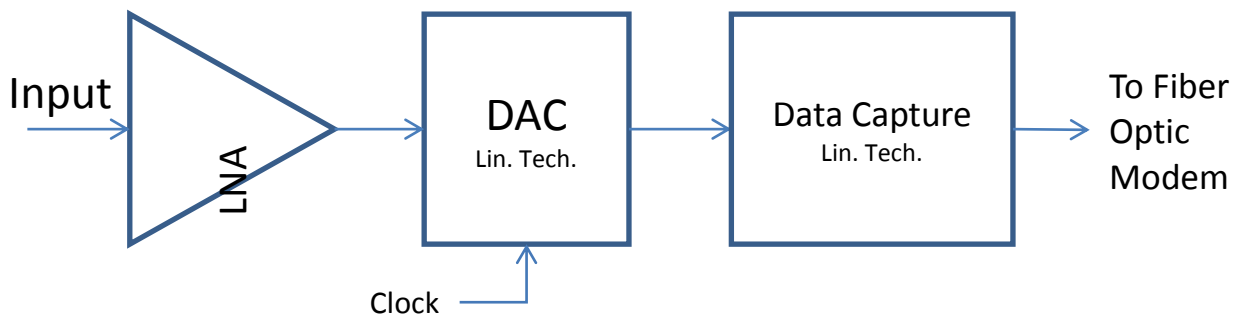


Figure 2 Receiver block diagram.

The transmitter and receiver containers were mounted on a steel frame, as shown in Figure 3.



Figure 3 Picture of the frame holding the transmitter (right) and the receiver (left) containers.

## **1.5 Field Data Collection and Verification**

The saltwater tank at the Northeastern University Marine Science Center was used for the preliminary experiment. That experiment was done using 8 single frequency signals between 100 kHz and 5 MHz and showed a reasonable match between what was expected and what was measured at ranges shorter than 70 cm.

To get away from the boundaries and build a solid frame of reference for a full-space model, the main experiment was carried out in the ocean at depth of around 5 m. (Skin depth at 100 kHz is approximately 0.77 m.) We did two sets of measurements. One was very close to the surface and the other one at roughly 5 m depth. The separation distance between the tips of the electrodes of the transmitter and the receiver was between 8 and 13 cm. We measured the conductivity of the water to be 4.3 S/m.

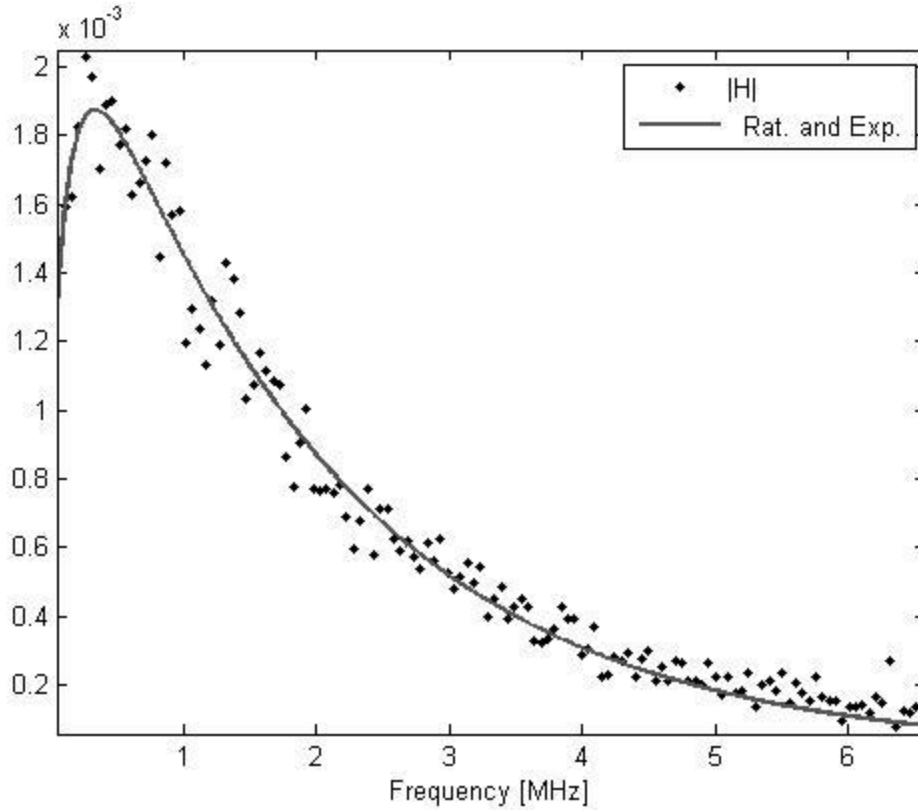


Figure 4 Magnitude of the CFR, measured at the surface.

Note that LNA gain  $G = 23.56$  dB was assumed in the calculation of the experimental CFRs shown in Figure 4 and Figure 5.

The rational and exponential fit in Figure 4 combines a rational and exponential function of frequency, in MHz, and it is given as

$$|H| = a \cdot \frac{p_1 f^2 + p_2 f + p_3}{q_1 f^2 + q_2 f + q_3} \cdot e^{-f/f_d}; \quad f_d \approx 1.94 \text{ MHz} \quad (10)$$

It shows a curvature in the channel transfer function around 400 kHz. (We see similar trend in Figure 5.) That is not completely unexpected considering the theory of electric dipole (Balanis, 1997); however, for the theory to be comparable to this particular curve, the separation distance between the transmitter and the receiver should be around 60 cm. Therefore, a more comprehensive model of the antenna system will be needed to provide better understanding of the propagation channel.

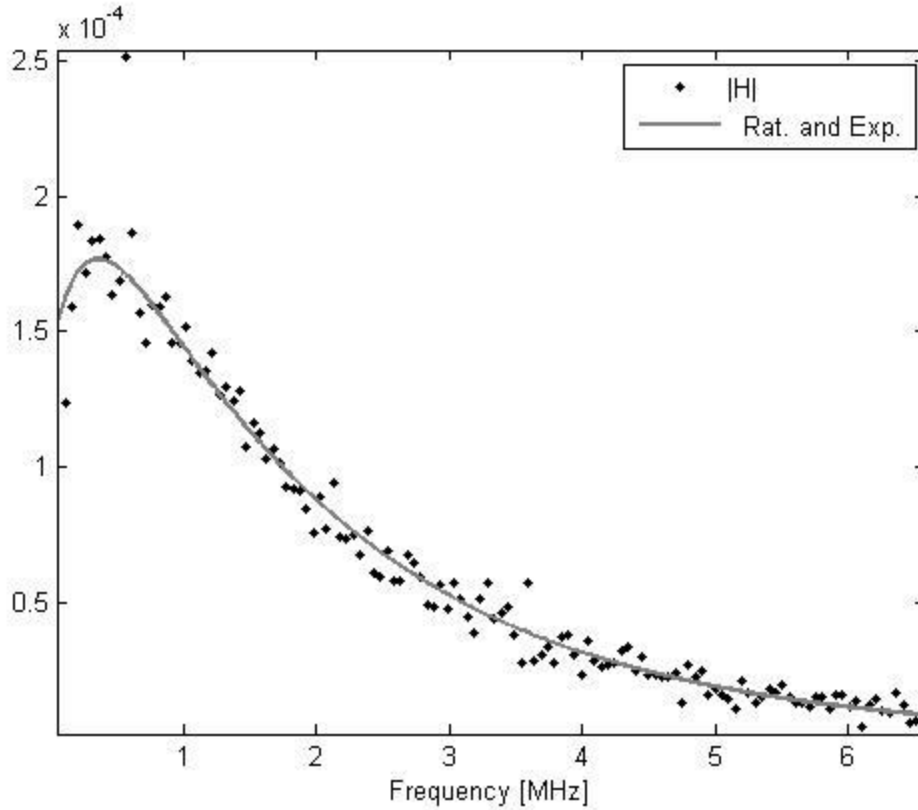


Figure 5 Magnitude of the Channel Transfer Function. Measurement was done at depth of roughly 5 m.

The rational and exponential fit in Figure 5 is characterized by

$$f_d \approx 2 \text{ MHz}$$

Phase characteristics in Figure 6 and Figure 7 show a minimum value between 3 MHz and 4 MHz. In case of theoretical electric dipole, that would indicate separation distance of a few cm. That is comparable to the distances we had in the experiment, although there is no clear definition of the distance in RF conduction method due to the fact that the transmission medium itself is used to convey electric current. By creating a more accurate model of our transmission system, we could generate more precise theoretical phase curves and use them to estimate the range.

The quadratic polynomial fit in Figure 6 is given by

$$\varphi(f) = 0.09f^2 - 0.58f + 0.15 \quad (11)$$

Frequency  $f$ , as before, is in MHz. Similarly, the quadratic polynomial fit in Figure 7 is given by

$$\varphi(f) = 0.09f^2 - 0.55f + 0.21 \quad (12)$$

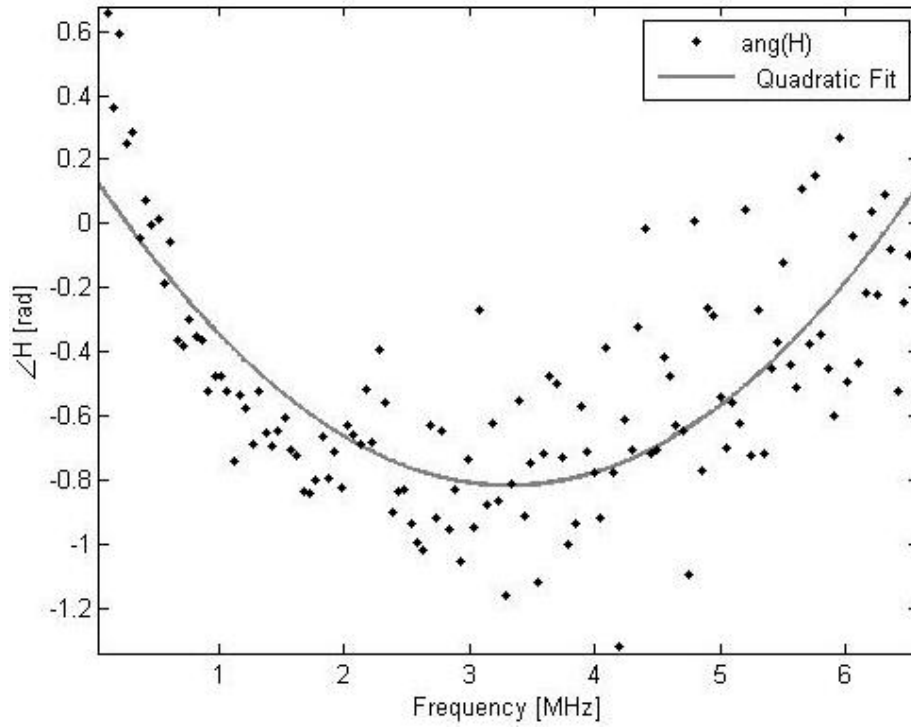


Figure 6 Phase at the surface.

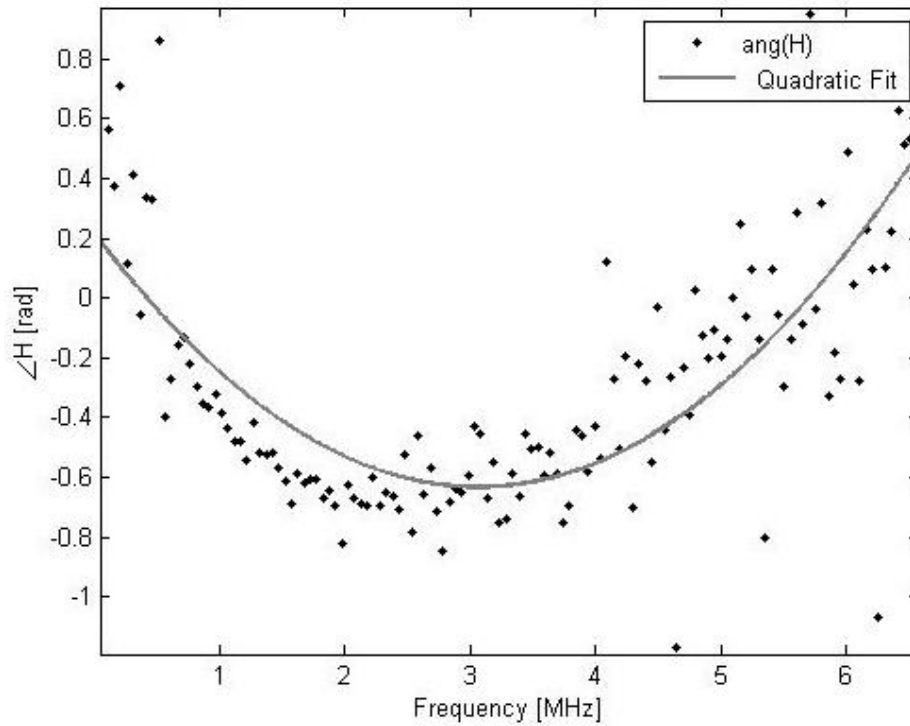


Figure 7 Phase at roughly 5 m depth.

## 1.6 Channel Capacity Assessment

Channel capacity of a discrete memory-less channel is the highest rate, in bits per transmission, information can be sent with arbitrarily low probability of error. Capacity of band-limited channel with Additive white Gaussian noise (AWGN), in bits per second, is given by (Cover, et al., 2006)

$$C = W \log \left( 1 + \frac{P}{N_0 W} \right) \quad (13)$$

Where  $P$  represents the signal power at the receiver,  $W$  is the frequency bandwidth of the channel and  $N_0$  is the power spectral density (PSD) of the noise.

To estimate capacity, we can use the signal attenuation, assessed in the previous section, and noise statistics.

In Figure 8 noise distribution looks similar to Normal, zero-mean Gaussian probability density function (PDF). Note that the statistics has been drawn based on limited amount of data available.

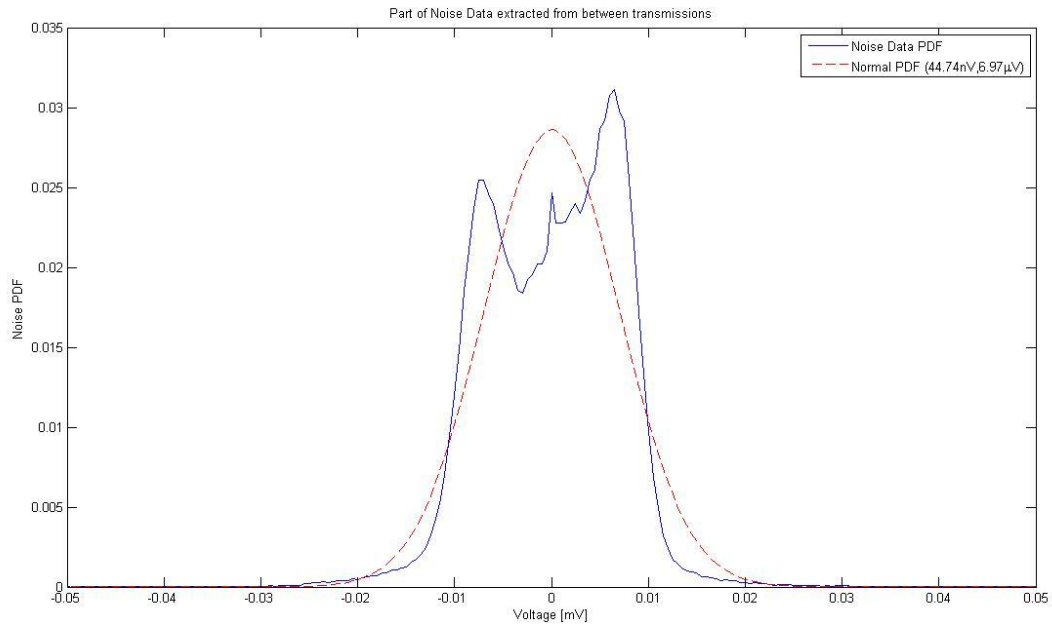


Figure 8 Noise PDF between 100 kHz and 6.35 MHz. Measured mean and standard deviation of the noise data were 44.74 nV and 6.97  $\mu$ V, respectively.

Capacity of parallel AWGN channels is a sum of the capacities of the individual channels (Cover, et al., 2006):

$$C = \sum_{i=1}^K \Delta W_i \log_2 \left( 1 + \frac{P_i}{N_0 \Delta W_i} \right) \quad (14)$$

Electromagnetic Noise PSD, between 100 kHz and 6.25 MHz, was estimated using the Burg parametric spectral estimation algorithm (Proakis, 2007). For the purposes of assessing the information capacity of the channel, we can approximate the noise PSD with a constant  
 $N_0 \approx 2.56 \cdot 10^{-20} \text{ W/Hz}$  (15)

Note that  $N_0$  corresponds to the input of the pre-amplifier, which in general is not part of the channel although it plays a very important role in signal detection. The measured data were collected at the output of the ADC module, as shown in Figure 2. Therefore, we had to convert the noise PSD from the output of the pre-amplifier to its input, based on the gain and noise figure of the specific component. Procedure for the corresponding noise level adjustment is given in (Egan, 2003).

$$N_{o,in} = \frac{N_{o,out}}{g R_{in}} - f_N k T_0 \quad (16)$$

In this expression,  $g$  represents the linear pre-amplifier gain, whereas  $f_N$  stands for the noise factor of the module that is used to adjust for the internal noise contribution of the pre-amplifier. The remaining parameters are the input resistance  $R_{in}$  and constant factor  $k T_0 \approx 4 \times 10^{-21} \text{ W/Hz}$ .

When communicating over parallel channels, total available power should be allocated across all channels optimally. By using the Lagrange multiplier optimization, it can be shown that optimum power allocation for parallel channels is achieved by applying so called water-filling method (Cover, et al., 2006). The optimization constraint is that the sum of sub-channel powers equals the total available power. If the channel is a collection of band-limited AWGN sub-channels centered on different sub-carriers, frequency dependent nature of transmission loss has to be factored in the power allocation.

For the attenuation shown in Figure 4 assuming total transmit power of 1 mW and 6.25 MHz bandwidth, the capacity is  $C_{1\text{mW}} \approx 64.6 \text{ Mbps}$  at the surface. For the deep measurement (Figure 5), which showed more attenuation than the surface measurement, the capacity is  $C_{1\text{mW}} \approx 25.6 \text{ Mbps}$ . That means we should be able to use more bits per symbol (higher order constellations) than BPSK and QPSK. Using OFDM, we can do non-uniform bit-loading across the carriers. Capacity is highly dependent on transmit power. For the deeper channel, respective capacities at 100 mW and 500 mW are  $C_{100\text{mW}} \approx 64 \text{ Mbps}$  and  $C_{500\text{mW}} \approx 78 \text{ Mbps}$ . These results are summarized in Table 1.

Power [mW]	1	100	500
Capacity [Mbps]	25	64	78

Table 1 Capacity of the channel in Figure 5 for three different transmit power values. Note that the capacity is expected to be significantly higher close to the ocean's surface and bottom due to boundary-reflected energy.

Our theoretical analysis has shown that expanding the total bandwidth at ranges shorter than 2 m could also result in significant data rate gain. Therefore, if a system is designed to operate at ranges longer than 2 m, capacity can be increased by a power increase. At ranges shorter than half a meter, by doubling the bandwidth the capacity virtually doubles. That could be a very useful result for some special applications in underwater communication systems where UWRF would eliminate the need for cumbersome or even implausible wiring and cabling over fixed links as short as just a few centimeters.

## **1.7 Data Demodulation and Detection**

As mentioned in the section on data transmission, we used BPSK and QPSK modulated sequences of OFDM symbols. From the data recorded at the surface, all BPSK modulated OFDM symbols could be detected with no error, even without channel estimation. Those symbols were used to estimate the channel state information (CSI) and apply it in the channel correction on the succeeding QPSK symbols (training method). That way, we were able to significantly lower the number of errors in the QPSK data detection. By using pilot tones, i. e. assuming some of the QPSK symbols within same OFDM symbol were known, we were able to further reduce the number of detection errors, but possibly at the expense of lower data rate.

With 16 pilots out of 128 subcarriers, we lose  $16/128 = 1/8$  of the bandwidth. In training mode, that sacrifice in data rate would be equivalent to using 1 out of 8 OFDM symbols for training. If the channel is fixed, training mode could use 1 out of more than 8 OFDM symbols for training. That would make the training mode more bandwidth efficient. Mean Square Distance (MSD) of the demodulated OFDM symbols from the known transmitted symbols in frequency domain can be used as a measure of detection reliability. MSE for each transmission is calculated as

$$MSD = \frac{1}{K} \sum_{k=1}^K \left( \frac{Y_k - U_k}{|U_k|} \right)^2 \quad (17)$$

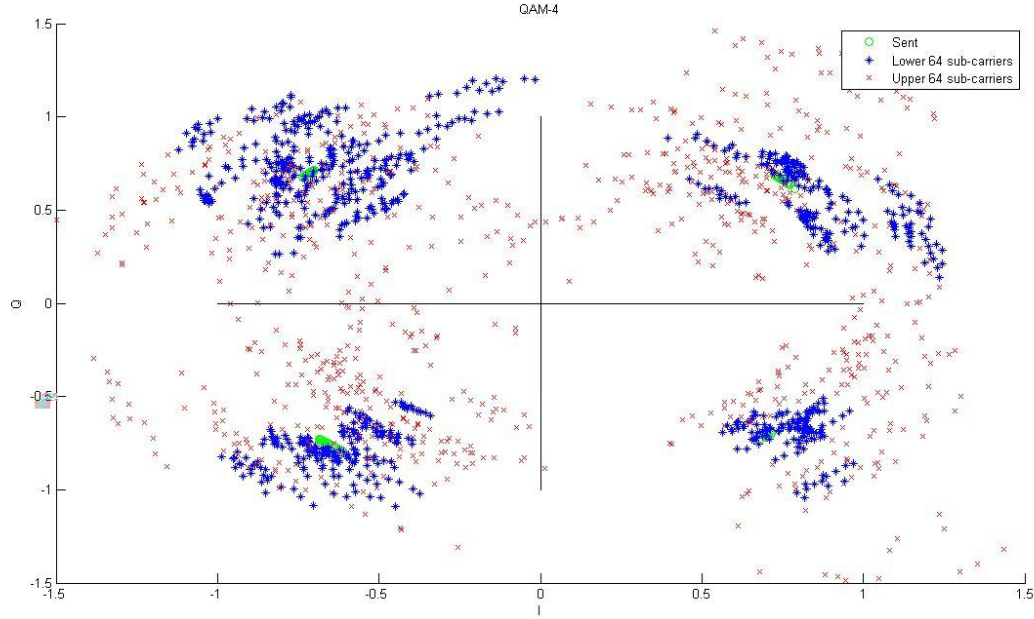


Figure 9 Training Mode at the surface. 14 transmissions. Symbol Error Rate (SER)=2.5%.  $\overline{MSD} = 0.19$ .

In (17),  $U_k$  and  $Y_k$  represent modulating and demodulated symbols, respectively, in frequency domain. Note that, for hardware related reasons, the transmitted symbols had to be converted to integers. That creates a little bit of distortion.

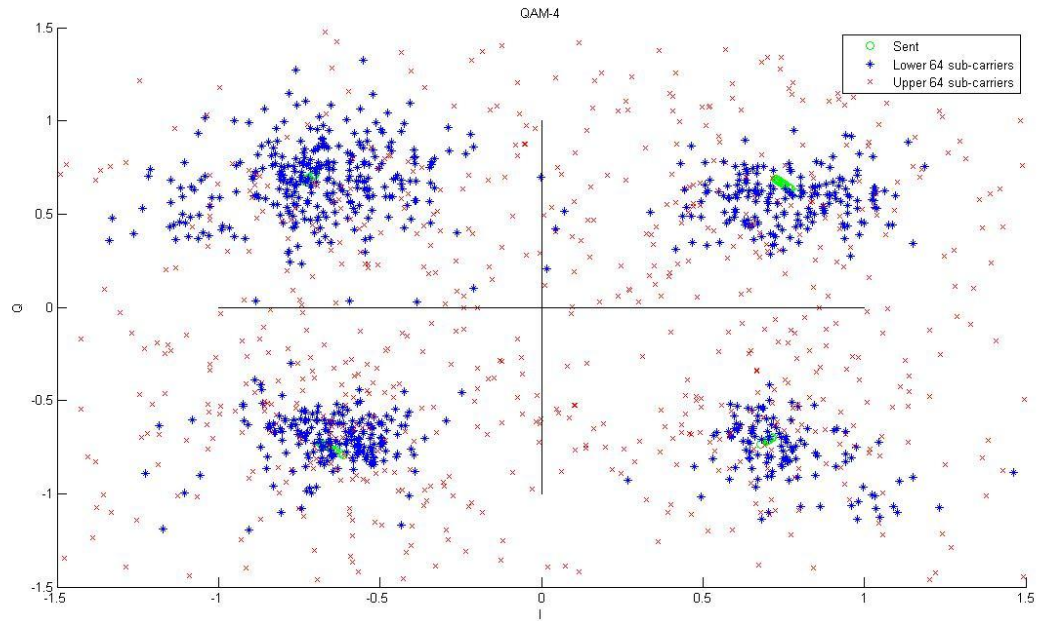


Figure 10 Training Mode at 5 m depth. 14 transmissions. SER=12.78%.  $\overline{MSD} = 1.14$ .

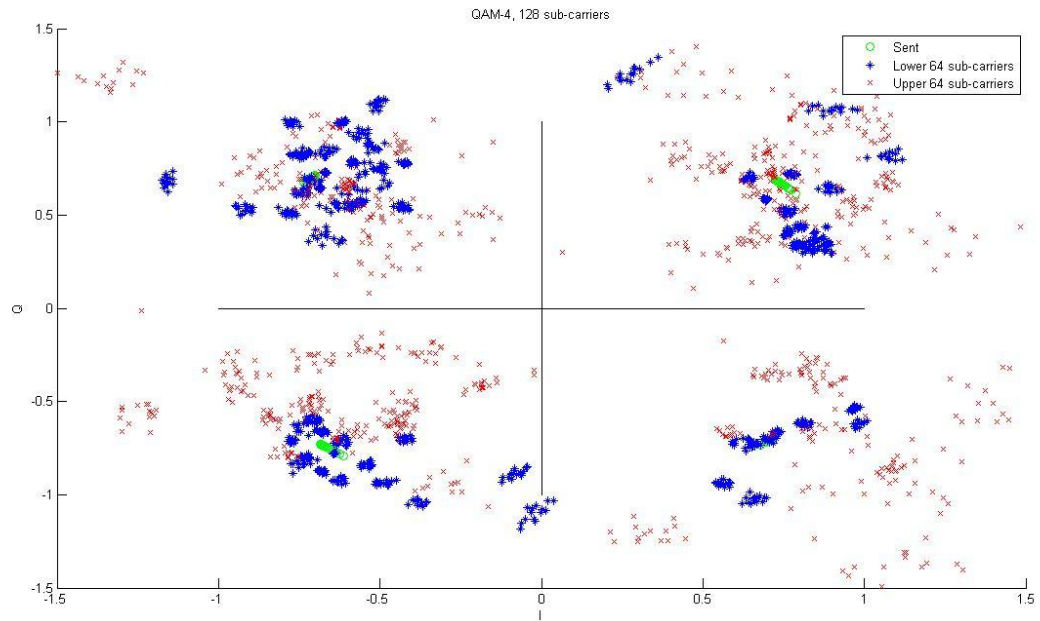


Figure 11 Pilot Mode at the surface. 16 pilots out of 128 subcarriers. Piece-wise linear interpolation between pilots. 14 transmissions. SER=0.7 %.  $\overline{MSD} = 0.16$ .

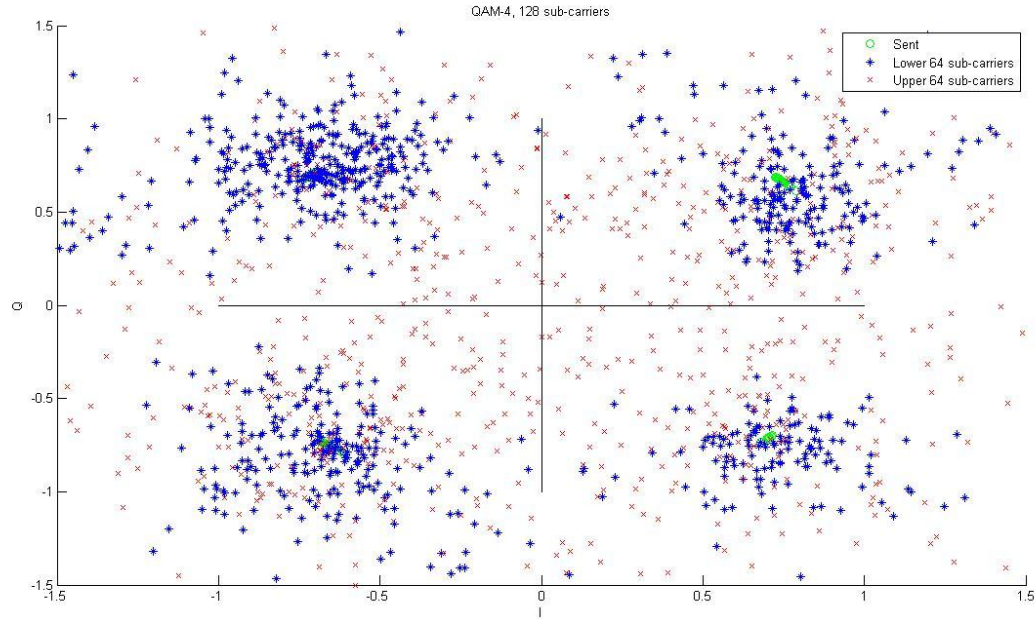


Figure 12 Pilot Mode at the 5 m depth. 16 pilots out of 128 subcarriers. Piece-wise linear interpolation between pilots. 14 transmissions. SER=15.88 %.  
 **$MSD = 1.7$ .**

## 1.8 Simulation Results

With the attained CFR models of the measured channels, we simulated an OFDM system with PSK modulation and either fixed or variable number of *bpsc*<sup>1</sup> in Matlab. Simulation environment gives us the flexibility of varying system parameters and testing different detection algorithms. Bandwidth of 6.25 MHz and 1024 subcarriers were used in simulations. Channel models are based on the sea test data analysis described above in the section Field Data Collection and Verification. AWGN channel and perfect channel estimation were assumed in simulations.

Figure 14 shows the Bit Error Rate (BER), as a function of normalized Signal to Noise Ratio (SNR), for a simulated OFDM system with fixed bpsc rate. The theoretical BER curves correspond to 64-PSK (6 bpsc) modulation (Sklar, 2006). Transmit power across the subcarriers was optimally allocated based on the water-filling method, while constant rate of 6 bpsc was used for each subcarrier. The channel model that corresponds to the BER in Figure 13a was the one shown in Figure 4, while the BER curves shown in Figure 13b correspond to the channel shown in Figure 5. One important observation in Figure 13 is that the deep water channel (Figure 4) has BER performance

<sup>1</sup> This term was introduced with respect to (9) to denote bits per subcarrier.

comparable to the surface channel (Figure 5), but at the cost of higher transmit power.

The channel coding was based on a convolutional encoder, with constraint length equal to 3, and Viterbi decoder (Viterbi, 1967). For  $E_b/N_0$  greater than 10dB, it can be seen in Figure 14 that the channel coding helped improve the BER. At the normalized SNR lower than 10dB channel coding actually seems to have increased the BER, which is not unexpected (Sklar, 2006).

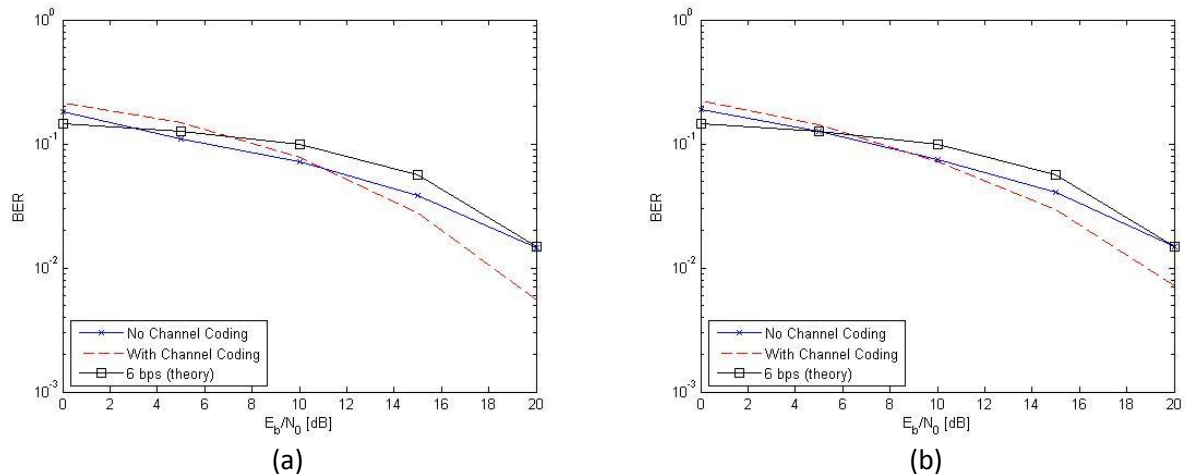


Figure 13 BER of fixed bps rate simulation results for 64-PSK with the two analyzed channel models, compared to the theoretical 64-PSK BER curve (Sklar, 2006). The channel models and the corresponding simulated transmit power for  $E_b/N_0=20\text{dB}$  are a) Surface channel (2mW) b) 5 m deep channel (165mW).

With variable bps rate, maximum 6 bps was allowed. The number of bps for each subcarrier was determined through the water-filling optimization method as mentioned in the section Channel Capacity Assessment. For  $E_b/N_0$  equal to 20dB, about 71% of the subcarriers were modulated with 6 bps, while 2 bps were allocated on about 10% of the subcarriers.

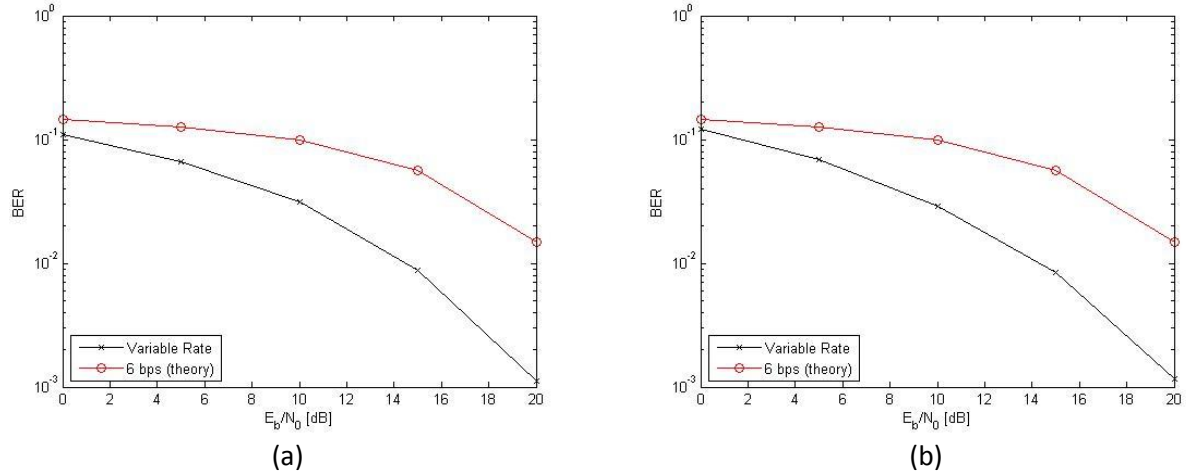


Figure 14 BER of the variable rate simulation through the analyzed channels (no channel coding), compared to the theoretical BER curve for 64-PSK. The channel models and the corresponding simulated transmit powers are a) Surface channel (2mW) b) 5m deep channel (165mW).

Figure 14 shows that the deep water channel (Figure 5) has BER performance comparable to the surface channel (Figure 4), but at the cost of higher transmit power.

With the variable rate transmission, given  $BER = 1e-3$  for  $E_b/N_0$  of 20 dB, the data throughput would be around 30 Mbps. Based on the expression (14), and with noise PSD given by (14), the capacity of these parallel Gaussian channels is  $C \approx 70$  Mbps. The assumed transmit power is 2mW for the surface channel and 165mW for the deep channel.

## 1.9 Documentation and Future Work

The results and findings of this project will be documented in a format suitable for publication and to support technology transfer. Although we carried out a comprehensive analysis of RF conduction that included propagation channel modeling and communication system simulation, the complexity of the problem is such that there are still significant improvement possibilities in our understanding of this communication channel.

On this project we limited our analysis to full-space, boundary-free, model of EM field propagation. That might not hold in reality. If an actual UWRF communication system is deployed in the vicinity of the surface or the bottom of the water column, boundary effects could play a significant role on the achievable data rates. By improving our understanding of the EM field propagation in various specific scenarios, we can continue to build a more complete picture of the capacity of UWRF channel. Power/bit allocation can be done at the transmit end to suit the channel. That way we can compare different bit loading and channel coding schemes that would bring us as close to the capacity as possible. If the range is very short, order of cm, we

can look into expanding the bandwidth to increase capacity. Roughly speaking, by doubling the bandwidth, at ranges shorter than half a meter, the capacity virtually doubles.

Theoretical model considered was the simple electric dipole. Electromagnetic (EM) Modeling of the sea water system consisting of two electrodes with opposite phase current could give better theoretical insight into the character of the propagation channel. We also noticed a difference in received signal level between electrode orientations when the transmitter and receiver electrode pairs point at each other and when they are parallel to each other. The parallel orientation seemed to give better reception. We will try to quantify that effect theoretically and experimentally.

With 128 frequencies, we were certainly able to draw a fairly detailed picture of the propagation channel vs. frequency. Increasing number of subcarriers to as high as 1024 or even higher would give us a benefit of having better channel estimation capabilities. That should be considered in the future. One of the limitations in regard to the number of subcarriers was the hardware. The OFDM symbols were hard-coded in VHDL for the FPGA. In a better fit hardware implementation, IFFT should be implemented in FPGA or a DSP processor.

The effect of imperfect channel estimation is important and should be analyzed. Moving into the simulation environment, we thought it would be better to first assume the channel attenuation and phase rotation are known at the receiver. Once we get the maximum out of a somewhat idealistic system, we can evaluate the impact of imperfect conditions.

Finally, we would also like to extend our analysis of the effectiveness of channel coding algorithms in the RF conduction channel, including combinations of various encoders. With the recent advances in modern communications techniques through advanced forms of modulation and channel coding we believe that communications through conduction can be a highly robust and viable mechanism without the limitations of other more commonly used techniques.

## **1.10 Acknowledgements**

This research was made possible by funding from RPSEA which was cost shared by GE Global Research and Northeastern University.

## **Bibliography**

**A. Shaw, A.I. Al-Shamma'a, S.R. Wylie, and D. Toal.** Experimental investigations of electromagnetic wave propagation in seawater. In Microwave Conference, 2006. 36th European, pages 572-575, Sept. 2006.

**R. Somaraju and J. Trumpf.** Frequency, temperature and salinity variation of the permittivity of seawater. Antennas and Propagation, IEEE Transactions on, 54(11):3441-3448, Nov. 2006.

**M.A. Chancey.** Short range underwater optical communication links. 2005.

**N. Fair, AD Chave, L. Freitag, J. Preisig, SN White, D. Yoerger, F. Sonnichsen, and W.H.O. Instn.** Optical modem technology for seafloor observatories. OCEANS 2006, pages 1-6, 2006.

**J.R. DePalma.** MARINE FOULING AND BORING ORGANISMS IN THE TONGUE OF THE OCEAN, BAHAMAS-EXPOSURE II, 1962.

**I.F. Akyildiz, D. Pompili, and T. Melodia.** Underwater acoustic sensor networks: research challenges. Ad Hoc Networks, 3(3):257-279, 2005.

**R.J. Urick.** Principles of Underwater Sound.(1983).

**A. Kaya and S. Yauchi.** An acoustic communication system for subsea robot. In OCEANS'89., pages 765-770, 1989.

**M. Chaplin.** Water structure and science. Available at:  
<http://www.lsbu.ac.uk/water/microwave.html>.

**Balanis C. A.** Antenna Theory: Analysis and Design [Book]. - New York : John Wiley & Sons, Inc., 1997.

**Che Xianhui [et al.]** Re-Evaluation of RF Electromagnetic Communication in Underwater Sensor Networks [Journal] // IEEE Communications Magazine. - 2010. - pp. 143-151.

**Cover T. M. and Thomas J. A.** Elements of Information Theory [Book]. - Hoboken, New Jersey : John Wiley & Sons, Inc., 2006.

**Egan William F.** Practical RF System Design [Book]. - Hoboken, New Jersey : John Wiley & Sons, Inc., 2003.

**Han Seung Hee and Lee Jae Hong** An Overview Of Peak-To-Average Power Ratio Reduction Techniques For Multicarrier Transmission [Journal] // IEEE Wireless Communications. - 2005. - pp. 56-65.

**Joe J. and Toh S. H.** Digital Underwater Communication Using Electric Current Method [Conference] // OCEANS. - 2007. - pp. 1-4.

**Momma H. and Tsuchiya T.** Underwater Communication by Electric Current [Conference] // OCEANS. - 1976. - pp. 631 - 636.

**Proakis John G.** Digital Signal Processing: Principles, Algorithms and Applications (3rd Edition) [Book]. - [s.l.] : Pearson Prentice Hall, 2007.

**Sklar Bernard** Digital Communications [Book]. - [s.l.] : Prentice Hall, 2006.

**Viterbi Andrew J.** Error Bounds for Convolutional Codes and an Asymptotically Optimum Decoding Algorithm [Journal] // IEEE Transactions on Information Theory. - April 1967. - Vol. IT13. - pp. 260-269.

**WFS** Seatooth [Online] // WFS Technologies Through-water and through-ground wireless technology. - WFS Technologies, 2011. - <http://www.wfs-tech.com/index.php/products/seatooth/>.

**Zhiqiang Wu, Jiadong Xu and Bin Li** A high-speed digital underwater communication solution using electric current method [Conference]. - [s.l.] : IEEE, 2010. - pp. V2-14 -V2-16.

## I. Appendix A

### Transmitter VHDL Code

```
library ieee;
use ieee.std_logic_1164.ALL;
use ieee.numeric_std.ALL;

entity memread is
port(
    SDRAM_DQ : in STD_LOGIC_VECTOR(31 downto 0);
    dout:out unsigned(15 downto 0); --output the data
    SDRAM_ADR_2o : out STD_LOGIC_VECTOR( 11 downto 0);
    SDRAM_BankAddr : out STD_LOGIC_VECTOR( 1 downto 0);
    SDRAM_ADR : out STD_LOGIC_VECTOR( 11 downto 0);
    MEMCON_DQ : in STD_LOGIC_VECTOR( 15 downto 0);
    SDRAM_BankAddr_2o : out STD_LOGIC_VECTOR( 1 downto 0);
    MEMCON_ADR : out STD_LOGIC_VECTOR( 30 downto 24);
    MAC_CSn : out STD_LOGIC;
    SDRAM_CASn_2o : out STD_LOGIC;
    SDRAM_FB_clk : in STD_LOGIC;
    CONSOLE_RX : in STD_LOGIC;
    CONSOLE_TX : out STD_LOGIC;
    SDRAM_CASn : out STD_LOGIC;
    SDRAM_WEn : out STD_LOGIC;
    SDRAM_DQM : out STD_LOGIC_VECTOR( 3 downto 0);
    SYS_Rst : in STD_LOGIC;
    SDRAM_RASn_2o : out STD_LOGIC;
    SDRAM_RASn : out STD_LOGIC;
    SDRAM_WEn_2o : out STD_LOGIC;
    FPGA_RESET_EN : in STD_LOGIC;
    BOOT_JP : in STD_LOGIC;
    syn_clk_o : out STD_LOGIC;
    MEMCON_WEn : out STD_LOGIC;
    nLED : out STD_LOGIC;
    SDRAM_Clk : out STD_LOGIC;
    MEMCON_OEn : out STD_LOGIC;
    SDRAM_Clk_2o : out STD_LOGIC;
    clk_in : in STD_LOGIC;
    MAC_INTERRUPT_IN : in STD_LOGIC);
end memread;

architecture fillmem of memread is
    component syn_clock
```

## Subsea Communications Final Report

08121-2902-03

```
    port ( CLKIN_IN      : in  std_logic;
          RST_IN        : in  std_logic;
          CLKFX_OUT      : out std_logic;
          CLKFX180_OUT   : out std_logic;
          CLKIN_IBUFG_OUT : out std_logic;
          LOCKED_OUT     : out std_logic);
end component syn_clock;
constant num_of_freq:integer := 128;
constant upsamp_factor:integer := 8;
constant symbol_size:integer := num_of_freq * upsamp_factor; -- fs not
exactly 50 MHz
constant cp_length:integer := symbol_size/8; -- cyclic prefix
constant sequence_size:integer := cp_length + symbol_size;
constant max_sequences:integer := 4; --2 bpsk and 1 qpsk and 2 64sc
--constant ramsize: integer := sequence_size * max_sequences;
type data is array (0 to sequence_size-1) of integer range 2**16-1 downto
0;
type RAMtype is array (0 to max_sequences-1) of data;

    constant    memr : RAMtype :=
(
--bpsk modulated sequence after IFFT and CP insertion (sequence_size)
( ),
--qpsk modulated sequence after IFFT and CP insertion (sequence_size)
( ),
--bpsk with 600kHz start (sequence_size)
( ),
--64 sc bpsk and qpsk (sequence_size)
( )
);
    signal clr, clk, lock: std_logic;
    signal sc4, sc5: std_logic;

begin

syn_clock1 : syn_clock port map(

                                clk_in,
                                clr,
                                clk,
                                sc4,
                                sc5,
                                lock);
```

**Subsea Communications Final Report**  
**08121-2902-03**

```
    clr <= SYS_Rst;
    syn_clk_o <= clk;

-- assign unused pins to quiet state
    SDRAM_Clk <= '0';
    SDRAM_RASn <= '0';
    SDRAM_CASn <= '0';
    SDRAM_WEn <= '1';
    SDRAM_DQM <= "ZZZZ";
    SDRAM_BankAddr <= "00";
    SDRAM_ADR <= "000000000000";
    SDRAM_Clk_2o <= '0';
    SDRAM_RASn_2o <= '0';
    SDRAM_CASn_2o <= '0';
    SDRAM_WEn_2o <= '1';
    SDRAM_ADR_2o <= "000000000000";
    SDRAM_BankAddr_2o <= "00";

    MEMCON_ADR <= "0000000";
    MEMCON_OEn <= '1';
    MEMCON_WEn <= '1';
    MAC_CSn <= '1';
-- SDRAM_FB_clk <= '0';
    CONSOLE_TX <= 'Z';

process(clk) is
    variable v,w,delaycounter,d: integer:=0;
begin
    -- insert code which uses memory data
    if clk'event and (clk='1') then
        if delaycounter=0 then
            dout <= to_unsigned(memr(w)(v),16);
            v := v + 1;
        end if;
        if v = sequence_size then delaycounter:=delaycounter + 1; end
    if;

        if delaycounter=sequence_size then delaycounter:=0; v:=0;
    w:= w + 1; end if;
        if w = max_sequences then w:=0; end if;
        d := d + 1;
        if d = 25*10**6 then -- toggle nLED every about 5s
            nLED <= not lock;
        elsif d = (25 + 5*50)*10**6 then
            nLED <= lock;
        end if;
    end if;
```

**Subsea Communications Final Report**  
**08121-2902-03**

```
        d:=0;  
    end if;  
end if;  
end process;  
end fillmem;
```

## I. Appendix B

### Pre-Processing MATLAB Code

```
fs_fm_ratio=2^3;
fs=51.6096e6; %Hz
fm=fs/fs_fm_ratio;
Ns=2^7; % Number of subcarriers
nSam=N*fs_fm_ratio; % number of Samples
cpLen=nSam/8; % cyclic prefix Length
df=fm/(N);
fL=df:df:fm;
Wl=2*pi*fL;
wL=Wl/fs;
fH=fm+df:df:fs/2;
wH=2*pi*fH/fs;
wNB=[wL wH];
Ffull=df:df:fs;
Wfull=2*pi*Ffull;
wFull=Wfull/fs;

Mu=4*pi*1e-7; %H/m
Eps0=1/(36*pi)*1e-9;
Epsr=81;
Eps=Eps0*Epsr;
Sigma=4; %m/s
EpsC=Eps-1i*Sigma./Wfull;

% Modulation
ConstellationSize=2^1; % 2^1=>BPSK
Modulation = modem.qammod(ConstellationSize); %QPSK spec.
case

% Channel
r=.25; %m Note: range=5mm=>all-pass
Io=5.5; %Ampere
f0=.1e6+.1e5; %10kHz shift (noise reason)
w0=2*pi*f0/fs;
GdB=29; %dB
G=10.^(GdB/20);
dl=.06; %m Dipole length
Theta=pi/2;

for seqcount=1:1
m(seqcount,:)=randint(1,N,ConstellationSize);
D = modulate(Modulation,m(seqcount,:));
u=ifft([D zeros(1,nSam-N)]);
```

## Subsea Communications Final Report

### 08121-2902-03

```

U=fft(u); ModU=abs(U);
n=1:numel(u);
ucp = [u(nSam-cpLen+1:nSam) u]; % add Cyclic Prefix
ncp=1:cpLen+nSam;
s(seqcount,:)=real(u.*exp(1i*w0*n)); %cos=1/2*(e+ + e-)
S=fft(s(seqcount,:)); ModS=abs(S);
scp(seqcount,:)=real(ucp.*exp(1i*w0*ncp)); %cos=1/2*(e+ +
e-)
k=Wfull.*sqrt(Mu*EpsC);
Eth=Io*d1./(4*pi*(Sigma+1i*Wfull*Eps))*sin(Theta)/r^3.*(1+1
i*k*r-k.^2*r^2).*exp(-1i*k*r);
H=Eth;
ModH=abs(H);
h=ifft(H);
hcp=ifft(H,numel(ncp));
ycp=cconv(scp(seqcount,:),real(hcp),numel(ncp));
ybb=ycp.*exp(-1i*w0*ncp); %down converted
% y=cconv(s(seqcount,:),real(h),numel(S));
y=ybb(cpLen+1:numel(ncp)); %remove CP
y=y*d1; %Voltage = Efield * Receiver Dipole Length
y=G*y; %Applying LNA gain at the receiver
Y=fft(y);

if seqcount<2,
figure,
plot(Ffull/1e6,ModS), hold
plot(Ffull/1e6,abs(Y),'r')
plot(Ffull/1e6,ModH,'k','linewidth',1.5)
axis([0 fs/2/1e6 0 1])
xlabel('frequency [MHz]'), ylabel('Spectrum Magnitude')
legend('Modulated sig.','Channel output',['Atten. (Io=',
num2str(Io) ,'A)'],'location','north')
title(['r=' num2str(r) 'm, f_0=' num2str(f0/1e6) 'MHz, BW='
num2str(fm/1e6) 'MHz=f_s/' num2str(fs_fm_ratio) ', Ncarr='
num2str(Ns) ', f_s=' num2str(fs/1e6) 'MHz'])
end %if
%Demodulation:
DeModulation = modem.qamdemod(Modulation);
yhat=ifft(Y./H); %phase derotation
uhat=yhat;
DHAT=fft(uhat);
if seqcount<2,
figure,
plot(real(Modulation.Constellation),imag(Modulation.Constel
lation),'or')
hold
plot(real(U(1:Ns)),imag(U(1:Ns)),'*k')

```

## Subsea Communications Final Report

### 08121-2902-03

```
plot(real(DHAT(1:Ns)), imag(DHAT(1:Ns)), 'x')
grid
xlabel('In-Phase'), ylabel('Quadrature')
legend(['Constellation-'
num2str(ConstellationSize)], 'Sent', 'Detected', 'location', 'SouthWest')
mhat=demodulate(DeModulation,DHAT(1:Ns));
SE=numel(find(mhat-m(seqcount,:)));
title(['Rx Gain=' num2str(GdB) 'dB; ' num2str(SE) '/'
num2str(Ns) ' Symb. Errs.'])
end %if
end

%Write samples
Maximums=max(abs(scp'));
for seqnum=1:numel(Maximums)
    scp(seqnum,:)=scp(seqnum,:)/Maximums(seqnum); %Even-up
end
sU = round(scp*(2^15-1))+2^15;
fid = fopen('tmpCp128bpsk.txt','w');
for seqwrnum=1:numel(Maximums)
    fprintf(fid, '(');
    wcount = fprintf(fid, '%05u, ',
sU(seqwrnum,1:length(sU)-1));
    fprintf(fid, '%05u),\n', sU(seqwrnum,length(sU)));
end
fprintf(fid, ')\n');
for rownum=1:numel(Maximums)
    fprintf(fid, '%d ',m(rownum,:));
    fprintf(fid, '\n');
end
fclose(fid);
```

## I. Appendix C

### Post-Processing MATLAB Code

```
% Script for Channel Frequency Response estimation
clc
clear
close all
fs=50e6;
Ns=2^7;
ConstellationSize=2^1; % 2^1=>BPSK
fs_fm_ratio=2^3;
f0=.1*1e6+.1e5;
w0=2*pi*f0/fs;
nsamt=N*fs_fm_ratio; %Tx fs nsam
nsam=round(nsamt*fs/51.6096e6); % fs_tx_fpga=51.6096e6;
cpLenT=nsamt/8;
cpLen=round(cpLenT*fs/51.6096e6); % fs_tx_fpga=51.6096e6;
roundingerror=((cpLenT+nsamt)*fs/51.6096e6-
(cpLen+nsam))/(cpLen+nsam);
pausesam=cpLen+nsam;
onerepsize=4*(cpLen+nsam+pausesam); %bpsk->pause->qpsk-
>pause
fileName='Depth1/Range1Snap2.adc';
Range=.09; %m
% fileName='Surface.adc';
% Range=.08; %m

fid = fopen(fileName, 'r');
for cnt=1:20
    a = fgetl(fid);
end
filereading = fscanf(fid, '%d');
fclose(fid);
Vpp=1.5; %dynamic range at the receiver
y=filereading'*Vpp/2/(2^15-1); clear filereading

% Modulation
Modulation = modem.qammod(ConstellationSize); %QPSK spec.
case
switch ConstellationSize
    case 2^1
        %bpsk
        load v; %bpsk symbols
        load s; %bpsk modulated waveform
    case 2^2
        %qpsk:
```

**Subsea Communications Final Report**  
**08121-2902-03**

```
        load v; %qpsk symbols
        load s; %qpsk modulated waveform
    end
    Vppt=2.00; %dynamic range at the transmitter
    s=s*Vppt/2/(2^15-1);

    %Demodulation:
    DeModulation = modem.qamdemod(Modulation);
    tcp=1:cpLen+nsam;
    errornum=ones(1,onerepsize)*Ns;
    for n=1:onerepsize,
        uhatcp=y(n:n+cpLen+nsam-1).*exp(-1i*w0*tcp); % to
    baseband
        uhat=uhatcp(cpLen+1:cpLen+nsam);
        DHAT=fft(uhat);
        mhat=demodulate(DeModulation,DHAT(1:Ns));
        errornum(n)=symerr(mhat,v);
    end
    [Min n1]=min(errornum);

    GdB=23.56; % Assumed LNA gain at Rx
    G=10.^(GdB/20); %Pre-amp gain at the receiver
    n2=n1;
    errornum2=[]; err2inds=[];
    dhatpdcouter=1;
    while n2+cpLen+nsam-1<numel(y)
        uhat2cp=y(n2:n2+cpLen+nsam-1).*exp(-1i*w0*tcp); % to
    baseband
        uhat2=uhat2cp(cpLen+1:cpLen+nsam);
        DHAT2=fft(uhat2)/nsam/G; %Gain adjustment included
        DHAT2PD=DHAT2(1:Ns); %no phase derotation
        mhat2=demodulate(DeModulation,DHAT2PD);
        errornum2=[errornum2 symerr(mhat2,v)];
    err2inds=[err2inds n2];
        M(dhatpdcouter,:)= DHAT2PD;
        dhatpdcouter=dhatpdcouter+1;
        n2=n2+onerepsize-3;
    end

    %scatter plot
    firstMrow=4;
    % lastMrow=size(M,1)-1;
    lastMrow=firstMrow;
    figure, hold
    for dhatpdcouter=firstMrow:lastMrow

        plot(real(M(dhatpdcouter,:)),imag(M(dhatpdcouter,:)),'*')
```

## Subsea Communications Final Report

### 08121-2902-03

```
%      Note: H=DHAT2PD./D=M(counter)./D;
end
plot([0 0], [min(min(imag(M))) max(max(imag(M)))], 'r')
plot([min(min(real(M))) max(max(real(M)))], [0 0], 'r')
xlabel('I'), ylabel('Q'),
title(['QAM-' num2str(ConstellationSize) ', ' num2str(Ns) '
sub-carriers'])
figure, plot(errornum2), title('Number of Bit Errors')
legend(['QAM-' num2str(ConstellationSize)])

%Plot H:
ttcp=1:cpLenT+nsamt;
fst=51.6096e6;
w0t=2*pi*f0/fst;
utcp=s.*exp(-1i*w0t*ttcp); % Tx seq. to baseband
ut=utcp(cpLenT+1:cpLenT+nsamt);
DHATt=fft(ut)/nsamt; % Tx DHAT
DHATtPD=DHATt(1:Ns); %no phase derotation
figure, %plot a part or the entire H matrix
H=M(firstMrow:lastMrow,:)./(ones(lastMrow-
firstMrow+1,1)*DHATtPD);
subplot(211),
freqCE=f0+[0:Ns-1]*fs/nsam; %fs=50MHz (Rx fs)
hold on
plot(freqCE/1e6, 20*log10(abs(H))'),
xlim([f0 freqCE(Ns)]/1e6)
xMarks=get(gca, 'xtick');
set(gca, 'xtick', [f0/1e6 xMarks])
xlabel('f [MHz]')
hold off
title(['QAM-' num2str(ConstellationSize) ...
', Range\approx' num2str(Range*100) ' cm'])
ylabel('|H|, dB'),
subplot(212),
% plot(freqCE'/1e6,
angle(H)./(ones(size(H,1),1)*2*pi*freqCE)),
% ylabel('\angleH/\omega')
plot(freqCE'/1e6, angle(H)/pi),
ylabel('\angleH/\pi')
xlim([f0 freqCE(Ns)]/1e6)
xMarks=get(gca, 'xtick');
set(gca, 'xtick', [f0/1e6 xMarks])
xlabel('f [MHz]')
title('Conductivity \sigma = 4.3 S/m')

capacity; % script that estimates capacity from attenuation
```